Annals of the Academy of Romanian Scientists
Physics Series
ONLINE ISSN 2066 – 8589 Volume 2, Number 1/2013

PERCOLATION PHENOMENA IN NETWORKS OF SILICON NANOCRYSTALS AND CARBON NANOTUBES

Magdalena Lidia CIUREA[1,2]

Abstract. *We discuss percolation phenomena in two nanostructures with percolative properties, one being formed by Si nanocrystals embedded in amorphous SiO_2 matrix and the second by a network of multi-walled C nanotubes embedded in amorphous Si_3N_4. This paper focuses on voltage percolation thresholds evidenced in current-voltage characteristics taken on both nanostructures. The shape of voltage percolation thresholds is common for both nanostructures and consists in a saturation plateau region of the current, followed by an abrupt increase.*

Key words: g percolation, electrical transport, silicon nanocrystals, carbon nanotubes

1. Introduction

The physical properties of nanostructures related to percolation phenomena are intensively investigated in the last decade. The main investigated are the nanostructures based on Si, Ge and C nanotubes (CNT), both single-walled (SWCNT) and multi-walled (MWCNT). Among the three basic percolation theories, the site percolation model describes well different characteristics, particularly the electrical ones [1]. The transport characteristics in electronic devices are also depicted by means of the bond percolation theory. If one considers a box with an infinite linear size, filled with both metallic balls with resistance R and plastic balls with infinite resistance, all of them having identical diameters, then the linear dimension (χ) of the largest clusters formed by interconnected metal balls is given by the formula $\chi \propto \chi_0 |x - x_c|^{-\nu}$. By χ_0 we noted the size of the ball, which generally represents a fundamental scale factor, by x and x_c the fraction and the critical fraction of metallic balls respectively, and ν = 0.88 is the universal critical index of the correlation radius for three dimensional systems [1, 2]. The numerical value of the critical fraction x_c depends on the balls arrangement, i.e. x_c has different values for a random or an ordered distribution. Also, x_c takes different numerical values for site percolation and bond percolation, respectively [1, 3].

[1]National Institute of Materials Physics, 105 bis Atomistilor Street, Magurele 077125, Romania (e-mail: ciurea@infim.ro);
[2]Academy of Romanian Scientists – Associate Member, 54 Splaiul Independentei, Bucharest 050094, Romania

The percolation phenomenon in a disordered system of nanocrystals embedded in an amorphous matrix explains the carrier transport by choosing optimal conduction paths which have minimum resistance. Thus, if the concentration of nanocrystals is higher than a critical value x_c , i.e. it is high enough to allow the carrier tunnelling, a charge current will be measured and this system is a percolative one. At a percolation site the electron chooses a path or another one, this being determined by the met potential barrier, which can be tunnelled or hopped. The dependence of percolation phenomena and conductance on nanocrystal concentration is frequently studied in literature, in a wide range of materials.

In this paper, two types of nanostructures are discussed, one consists of Si nanocrystals (nc-Si) embedded in amorphous SiO_2 (a-SiO_2) matrix (Si-SiO_2 system) and the second is formed by MWCNT network embedded in amorphous Si_3N_4. The electrical, photoelectrical and optical properties of Si-SiO_2 systems obtained by magnetron sputtering related to their microstructure were intensively investigated [4-7]. These films are formed by nc-Si or noncrystalline Si and SiO_2 islands [4, 5, 8-12]. Electrical transport and photoluminescence properties of films with different nc-Si volume concentration (x) were studied [5, 7]. The authors found that the dominant transport mechanism is migration bellow x_c, Coulomb blockade at x_c and tunnelling above x_c, respectively [5]. The dark conductivity and photoconductivity curves depend on nc-Si concentration after a power law $\sigma \propto (x - x_c)^t$, with $t \approx 2$, typical for percolation behaviour. The ultrafast carrier conduction in films of nc-Si embedded in a SiO_2 matrix with various nc-Si contents was studied by using time-resolved terahertz spectroscopy [13]. The conductivity at zero-frequency σ_0 was found to follow the $\sigma_0 \propto (x - x_c)^\gamma$ scaling law, with $x_c \approx 38$ % and $\gamma \approx 1$.

As in the case of Si-SiO_2 system, the electrical conductivity σ of the CNT-based composites depends on the CNT content, sizes and type (SWCNT, MWCNT) [14-16]. Both SWCNTs and MWCNTs can have metallic or semiconductor behaviour, MWCNTs being always electrically conductive even at low temperatures. The MWCNT-based systems have a percolative behaviour, so that the conductivity abruptly increases when the MWCNT volume concentration x_{MWCNT} or mass fraction - f_{MWCNT} becomes close to x_c or f_c, respectively [15, 17, 18]. The dependence of conductivity σ on x_{MWCNT} follows a power law $\sigma \propto (x_{MWCNT} - x_c)^t$, with t the critical exponent, which is typical for percolation behaviour [14, 15, 17, 19]. Various values for x_c (f_c) and σ were reported in literature, they depending on CNT sizes, and also if CNTs are single, multi-walled or even bundles [15].

By investigating dc electrical conductivity and dielectric properties of the MWCNT-alumina composites, a sharp increasing of the conductivity with eight

orders of magnitude at the percolation threshold of 0.79 was observed [20, 21]. The critical exponent was found to have a value between the theoretical values corresponding to 2D (1.33) and 3D (1.94). In MWCNT-Si_3N_4 composites sintered by spark-plasma an increase of σ with about ten orders of magnitude was observed, a power low of σ with x_{MWCNT} was evidenced, with $t \approx 1.73$ at $x_c \approx 0.64$ vol % [17].

This paper focuses on results and discussions concerning voltage percolation thresholds in two nanostructures with percolative properties, one being formed by nc-Si embedded in a-SiO_2 matrix (Si-SiO_2 system) and the second by MWCNT network embedded in amorphous Si_3N_4. The voltage percolation thresholds were evidenced in current-voltage ($I - V$) characteristics taken on both nanostructures.

2. Preparation and structure investigations

The Si-SiO_2 films were prepared by co-sputtering Si and SiO_2 on quartz substrates [4, 8, 22], followed by an annealing in N_2 at 1100 ^oC for nanostructuring. These films are formed by nc-Si embedded in an amorphous SiO_2 matrix. Thus, samples with variable volume concentration (from $x \approx 0$ % to $x \approx 100$ %) from the one end to the opposite one are obtained, while the mean nanocrystal diameter varies slowly with x. For electrical measurements, 50 planar, parallel Al electrodes (2 mm width) were thermally deposited.

The measurements were performed on samples formed between any two neighbour electrodes, these samples having different nc-Si concentrations. High resolution transmission electron microscopy (HRTEM) investigations performed in a region with the nc-Si concentration of $x \approx 50$ % evidence nc-Si (Si nanodots) embedded in an amorphous SiO_2 matrix (Figure 1), tending to form chains separated by a-SiO_2. So, microstructure investigations reveal that the Si-SiO_2 structure is a percolative system [23, 24] and therefore it is to be expected that percolation processes govern the electrical transport.

The MWCNT-Si_3N_4 structures were prepared in a sandwich geometry (quartz/Cr/Al/MWCNT-Si_3N_4/Cr/Al) [24-26], as it is shown in the sketch illustrated in Figure 2. The MWCNTs were embedded in Si_3N_4 by the plasma enhanced chemical vapour deposition. Then, the Si_3N_4 layer was etched in order to uncover the ends of MWCNTs. The cross-sectional TEM made on MWCNT-Si_3N_4 structures showed that this structure has a fibrous morphology. A similar investigation made onto a carbon – copper TEM grid on which the nanotubes are directly pipetted demonstrated that MWCNT network is uniformly and homogeneously embedded in the amorphous Si_3N_4 matrix [26].

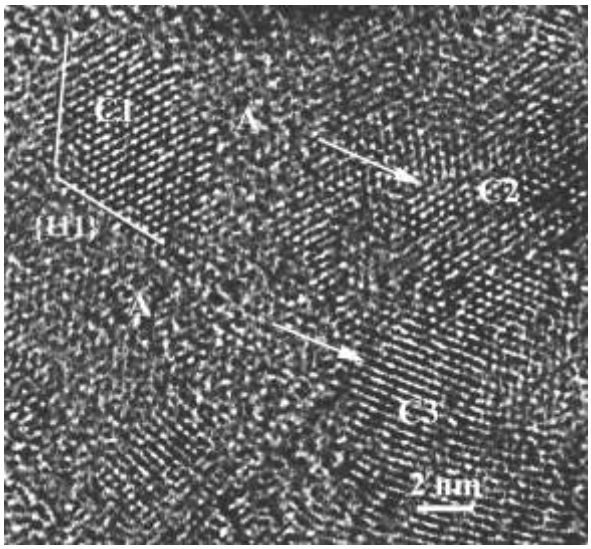

Figure 1. HRTEM image of Si – SiO_2 films ($x \approx 50$ %). C1 to C3 are Si nanocrystals and A is a-SiO_2 matrix. The fringes show the relative orientation of the nanocrystals [27].

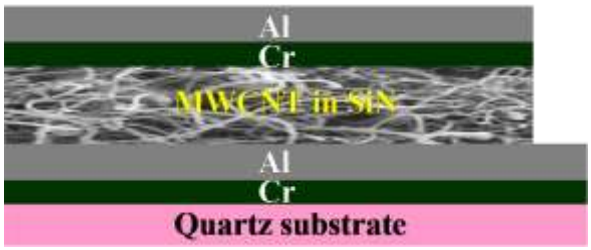

Figure 2. Quartz/Cr/Al/MWCNT-Si_3N_4/Cr/Al sandwich structure.

3. Results and discussions

The current–voltage (I – V) characteristics at room temperature (RT), taken on samples with various nc-Si concentrations are presented in Figures 3, 4 and 5.

The insert in Figure 3 allows to determine the percolation threshold in concentration being $x_t \approx 34.7$ % (the mean value of the two concentrations) [24, 27]. Indeed, at $x \approx 33.7$ %, the noise is of the same order of magnitude ($2 \cdot 10^{-8}$ A) as the current at 2 V bias, while at $x \approx 35.7$ %, the current is one order of magnitude greater. The 2 V bias was chosen as test value because the Coulomb blockade energy in nanodots with diameters between 4 and 6 nm is 38 – 58 meV. A previous investigation of the I – V characteristics, made at $x \approx 66$ % [4, 24], proved that the Coulomb blockade at RT is 1.75 V. As the Coulomb blockade threshold is roughly proportional with the cubic root of the number of

nanocrystals, it means that its value at $x \approx 34.7$ % is about 1.4 V. Then the limitation of the bias under 2 V in search of the percolation threshold is covering.

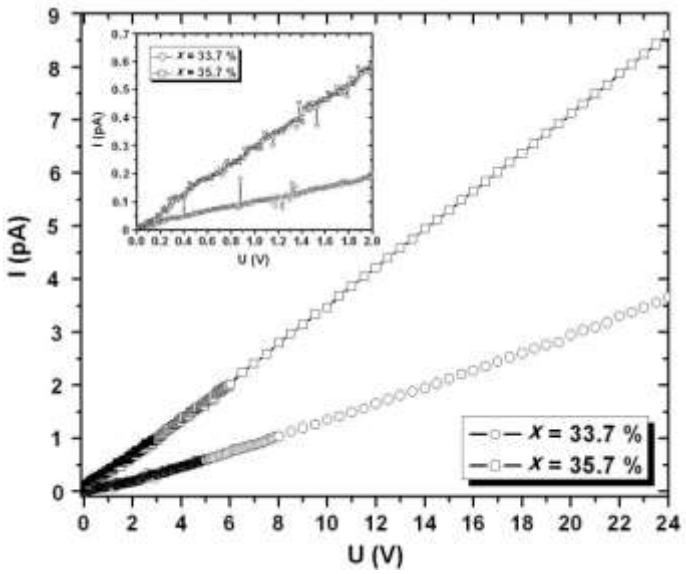

Figure 3. *I – V* characteristics around the percolation threshold ($x_t \approx 34.7$ %) [27].

Near x_c the *I – V* curves present a linear behaviour [28]. Similar values of the concentration percolation threshold in Si-SiO_2 systems were reported in literature. In the Refs. [5, 13] the reported value of the concentration percolation threshold is $x_c \approx 38$ %.

The measurements made at two intermediate nc-Si concentrations are presented in Figures 4 and 5. One can see that the current is two orders of magnitude greater and the characteristics are no more linear, but they are dominated by the high field assisted tunnelling mechanism [4, 24, 28, 29]:

$$I = I_0 \operatorname{sign}(U)\left[\left(1-|U|/U_0\right)\times\exp\left(-\alpha\sqrt{1-|U|/U_0}\right)-\exp(-\alpha)\right], \quad (1)$$

where $U_0 = N\varphi/e$, $\alpha = \delta\chi\varphi^{1/2}$ and $\chi = (8m^*/\hbar^2)^{1/2}$ (m^* is the effective carrier mass inside the nanocrystal and N the mean number of tunnelled barriers of height φ and width δ). By fitting *I – V* curves measured on samples with different nc-Si concentration with Equation 1, and taking for the potential barrier height the value experimentally determined, $\varphi = (2.2 \pm 0.2)$ eV and for the mean barrier width 1.7 nm, one obtains the number N of tunnelled barriers in the range 64 and 126. This number is small because, with the increase of x, the number of equivalent paths having lower resistance sharply increases. In other words, one has to keep in mind that the estimated number of tunnelled barriers does not represent the total number

of barriers existing in the sample between the electrodes. Some of barriers are short-circuited by the electrons that find less resistive paths.
If one analyses *I* – *V* curves from Figure 4 measured on samples with 39.8 % and 43.9 % nc-Si, several percolation thresholds (marked by arrows) appear at 16 and 18 V only for $x \approx 39.8$ %, and at 17.2, 19.1, 20.6 and 22.1 V for both, $x \approx 39.8$ % and $x \approx 43.9$ %. These thresholds are related to the possibility of tunnelling larger barriers with the increase of the bias. It is remarkable that the higher voltage thresholds are practically the same for the two concentrations. All these percolation thresholds have a similar shape, namely a saturation plateau followed by an abrupt increase of the current. Also, this shape is independent on the nc-Si concentration as the curves in Figure 4 demonstrate.

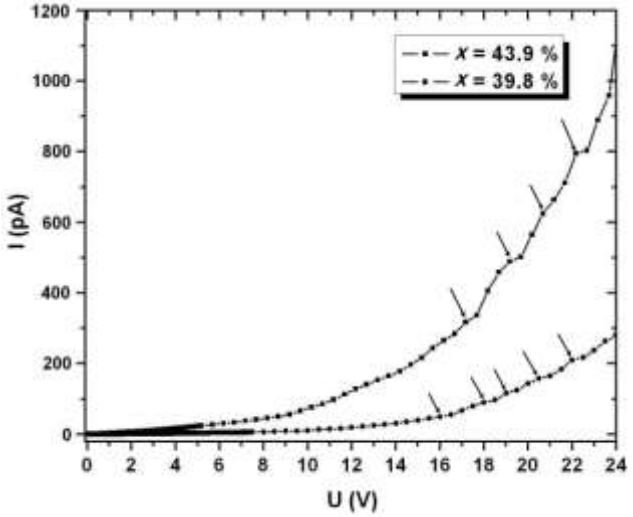

Figure 4. *I* – *V* characteristics at nc-Si concentrations of 43.9 and 39.8%.
The arrows mark voltage percolation thresholds [27].

The voltage percolation thresholds, evidenced in the *I* – *V* curves in Figure 4 are related to the random distribution of the Si nanocrystals [27], so that, at each voltage percolation threshold, new (less resistive) paths are opened for the carriers. Consequently, the increase of the applied voltage opens new paths by tunnelling larger barriers and therefore the current abruptly increases. At high enough nc-Si concentration, all available paths are opened and Equation 1 becomes rigorous. Thus, looking at the *I* – *V* characteristic in Figure 5, taken on a sample with a nc-Si concentration of 94.89 %, one can observe the disappearance of the percolation thresholds.

In general, in a percolative system with a linear *I* – *V* characteristic, the conductance depends on the concentration by a power law. Si-SiO_2 system presents a superlinear *I* – *V* curve, so that the initial differential conductance (G_0), defined as $G_0 = (dI/dV)_{V=0}$, has to be evaluated as function of the nc-Si

concentration. It was found that G_0 follows the power law $G_0 \propto (x - x_c)^{\gamma}$, with the critical exponent $\gamma = 0.88$ [27]. It is remarkable that this dependence extends

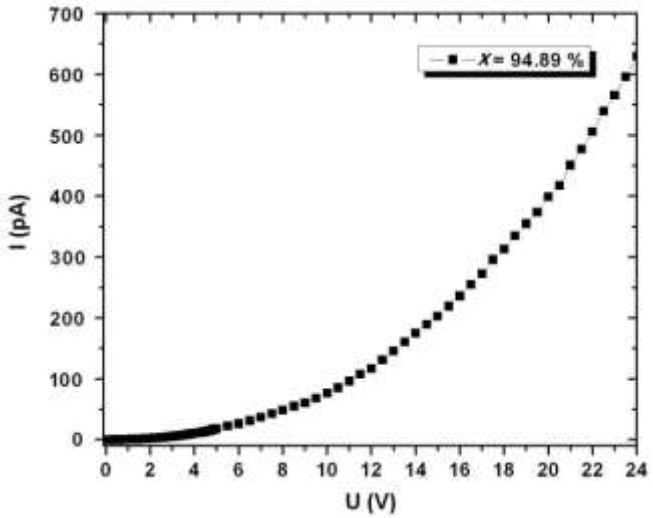

Figure 5. *I – V* characteristic at high nc-Si concentration [27].

from the Ohmic to the high field assisted tunnelling behaviour. This proves that the percolative behaviour does not depend on the local transport mechanism, but only on the nanodots distribution. Titova *et al.* [13] showed that the zero-frequency conductivity σ_0 also follows the $\sigma_0 \propto (x - x_c)^{\gamma}$ scaling law with $\gamma \approx 1$. In the literature one finds $G \propto (x - x_c)^{t}$ with $t \geq 2 \neq \gamma$ [5]. The conductivity of an infinite system in 3D is $\sigma \propto (x - x_c)^{2}$ [1]. From Equation 1 one obtains for G_0:

$$G_0 = \frac{I_0}{U_0}\left(\frac{\alpha}{2} - 1\right)\exp(-\alpha). \tag{2}$$

One has to remark that $\exp(-\alpha)$ is proportional with the tunnelling probability (P_t) and this is proportional with the percolation probability (P_p), so that:

$$G_0 \propto P_t \propto P_p \propto (x - x_c)^{\nu} \tag{3}$$

Consequently, the critical exponent γ is related to the tunnelling probability and is identified with the critical exponent for percolation probability (ν). In the literature the exponent corresponding to a tunnelling process is reported to be $\nu \approx 0.88$, in good agreement with $\gamma \approx 0.88$. The value found for the critical exponent is close to the critical exponent previously found for nanocrystalline porous silicon ($\gamma \approx 0.88$) [28].

In order to evidence the percolative behaviour of MWCNT-Si_3N_4 nanostructures, they were electrically investigated by measuring *I – V* characteristics at both low

and high temperatures, i.e. at 20 K and RT 298 K. As one can see in Figure 8, *I* –*V* dependence is linear for both curves showing a metallic-like behaviour of these structures. The linear dependence of the resistance-temperature curve was also observed in the literature [25]. In the Ref. [17], *I* – *V* characteristics on MWCNT-Si_3N_4 composites were measured at different temperatures between 323 and 573 K. The authors evidenced both semiconductor and metallic-like behaviours, mainly depending on the MWCNTs content. Thus, for samples with low content of MWCNT, *I* – *V* characteristics present a non-linear behaviour, σ increasing with *T*, typical for a semiconductor behaviour. Also, the authors proposed a hopping or tunnelling mechanism across/through potential barriers between MWCNTs and across atomic defects formed within the nanotubes if they are twisted and bended. For structures with high x_{MWCNT}, the *I* – *V* dependence is linear at relatively low temperatures (up to 423 K) and non-linear at higher temperatures. A metallic-like conduction related to the charge transport along the nanotube shells was also evidenced.

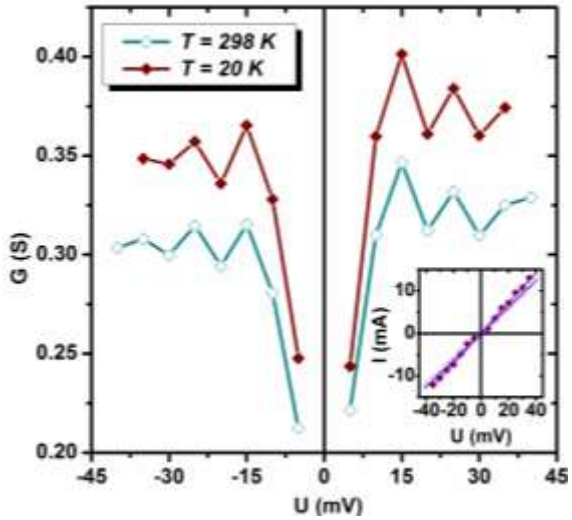

Figure 6. The *G* – *V* curves at 20 and 298 K.
In the insert are given *I* – *V* curves measured at 20 and 298 K.

As one can see from the insert in Figure 6, *I* – *V* characteristics are linear, presenting small oscillations around the linear fit ($G \approx 0.31$ S for $T = 298$ K, $G \approx 0.36$ S for $T =$ 20 K). The conductance-voltage ($G - V$) curves show maxima and minima at the same voltages on both curves (Figure 6). These maxima and minima are symmetrical in bias polarization, they are not periodic and do not depend on temperature. Consequently, these oscillations can not be attributed to the Coulomb blockade effect. In our opinion, in the disordered MWCNT network, they are related to percolation processes which are due to the field-assisted tunnelling between adjacent MWCNTs embedded in the amorphous Si_3N_4 matrix. The current oscillations can be explained as follows: the current increases with the voltage increase up to a limit determined by

the conduction quantification in the metallic nanotubes, and consequently, the $I - V$ curves become sublinear and a conductance minimum is reached. Then the electric field will increase up to the voltage percolation threshold, the tunnelling probability will increase and less resistive paths will be opened. Consequently the $I - V$ characteristic becomes superlinear and the conductance becomes maximum. The voltage percolation thresholds of 20 and 30 mV corresponding to the conductance minima on both bias polarities and temperatures (20 and 298 K) are evidenced (Figure 6). In MWCNT-polymer composite, a conduction model consisting in tunnelling of electrons through the polymer between the interconnected MWCNTs was proposed [21].

Conclusions

In this paper, the voltage percolation thresholds with the same shape, meaning a saturation plateau of the current, followed by an abrupt increase, were evidenced in the $I - V$ characteristics measured on two nanostructures, one being formed by nc-Si embedded in a-SiO_2 matrix and the second by MWCNT network embedded in amorphous Si_3N_4.

In Si-SiO_2 films, the voltage percolation thresholds are due to tunnelling through potential barriers generated by SiO_2 between neighbouring Si nanocrystals. The critical exponent (0.88) for initial differential conductance was identified with the exponent for tunnelling probability and the critical exponent for the percolation probability, too. Consequently, the electrical transport in Si-SiO_2 films with random space distribution of Si nanocrystals is percolative.

Similarly with the Si-SiO_2 films, MWCNT network embedded in Si_3N_4, displayed oscillations (maxima and minima) in the $G - V$ and $I - V$ curves, which are determined by percolation processes. These maxima and minima are symmetrical in bias polarization, they are not periodic and do not depend on temperature. The voltage percolation thresholds of 20 and 30 mV corresponding to the conductance minima on both bias polarities and temperatures (20 and 298 K) are evidenced. The analysis of the voltage percolation thresholds in the $G - V$ and $I - V$ curves represents an original approach to the study of the percolation phenomena in Si-SiO_2 and MWCNT- Si_3N_4 nanostructures.

This model can be applied to any other nanostructure containing random distribution of nanocrystals or nanotubes embedded in an insulating and/or amorphous matrix.

Acknowledgment

I am deeply indebted to Ionel Stavarache, Ana-Maria Lepadatu, Valentin Serban Teodorescu, Mircea Dragoman, George Konstantinidis, Raluca Buiculescu because a part of the research work briefly overviewed in this paper has been carried out in collaboration with them.

REFERENCES

[1] Hunt, Complexity **15**, 8 (2009).

[2] M. Aroutiounian, M. Zh. Ghulinyan, Phys. Stat. Sol. (a) **197**, 462 (2003).

[3] D. Stauffer, Classical Percolation, Lect. Notes. Phys. **762**, 1 (2009).

[4] M. L. Ciurea, V. S. Teodorescu, V. Iancu, I. Balberg, Chem. Phys. Lett. **423**, 225 (2006).

[5] I. Balberg, E. Savir, J. Jedrzejewski, A. G. Nassiopoulou, S. Gardelis, Phys. Rev. B **75**, 235329 (2007).

[6] O. Wolf, O. Millo, I. Balberg, J. Appl. Phys. **113**, 144314 (2013).

[7] S. Ilday, H. Ustunel, F. Ö. Ilday, D. Toffoli, G. Nogay, D. Friedrich, R. Hübner, B. Schmidt, K.-H. Heinig, R. Turan, arXiv:1309.4400 [cond-mat.mtrl-sci] (2013).

[8] V. S. Teodorescu, M. L. Ciurea, V. Iancu, M.-G. Blanchin, J. Mater. Res. **23**, 2990 (2008).

[9] M. L. Ciurea, V. Iancu, V. S. Teodorescu, L. C. Nistor, M. G. Blanchin, J. Electrochem. Soc. **146,** 3516 (1999).

[10] M. L. Ciurea, M. Draghici, V. Iancu, M. Reshotko, I. Balberg, J. Luminesc. **102-103**, 492 (2003).

[11] B. Urbach, E. Axelrod, A. Sa'ar, Phys. Rev. **B** 75, 205330 (2007).

[12] M. L. Ciurea, V. Iancu, Proc. IEEE CN 00TH8486, Int. Semicon. Conf. CAS 2000, Vol. **1**, 55 (2000).

[13] L. V. Titova, T. L. Cocker, D. G. Cooke, X. Wang, Al Meldrum, F. A. Hegmann, Phys. Rev. B **83**, 085403 (2011).

[14] B. E. Kilbride, J. N. Coleman, J. Fraysse, P. Fournet, M. Cadek, A. Drury, S. Hutzler, S. Roth, W. J. Blau, J. Appl. Phys. **92**, 4024 (2002).

[15] K. Ahmad, W. Pan, S.-L. Shi, Appl. Phys. Lett. 89, 83122 (2006).

[16] W. S. Bao, S. A. Meguid, Z. H. Zhu, Y. Pan, G. J. Weng, J. Appl. Phys. **113**, 234313 (2013).

[17] J. González-Julián, Y. Iglesias, A. C. Caballero, M. Belmonte, L. Garzón, C. Ocal, P. Miranzo, M. I. Osendi, J. Compos. Sci. Technol. **71**, 60 (2011).

[18] B. De Vivo, P. Lamberti, G. Spinelli, V. Tucci, J. Appl. Phys. **113**, 244301 (2013).

[19] I. Balberg, D. Azulay, Y. Goldstein, J. Jedrzejewski, G. Ravid, E. Savir, Eur. Phys. J. B **86**, 428 (2013).

[20] D. Stauffer, Introduction to the percolation theory. London and Philadelphia: Taylor & Francis (1985).

[21] C. Gau, C.-Y. Kuo, H. S. Ko, Nanotechnol. **20**, 395705 (2009).

[22] V. S. Teodorescu, M. L. Ciurea, V. Iancu, M. G. Blanchin, Proc. IEEE CN 04TH8748, Int. Semicond. Conf. CAS 2004, Vol. **1**, 59 (2004).

[23] Y.-M. Lee and Y. Wu, Appl. Surf. Sci. **254**, 4591 (2008).

[24] I. Stavarache, Digest J. Nanomater. Bios. **6** (3), 1073 (2011).

[25] M. L. Ciurea, I. Stavarache, A.-M. Lepadatu, V. Iancu, M. Dragoman, G. Konstantinidis, R. Buiculescu, Proc. IEEE CN CFP09CAS-PRT, Int. Semicon. Conf. CAS 2009, Vol. **1**, 121 (2009).

[26] I. Stavarache, A.-M. Lepadatu, V. S. Teodorescu, M. L. Ciurea, V. Iancu, M. Dragoman, G. Konstantinidis, R. Buiculescu, Nanoscale Res. Lett. **6**, 88 (2011).

[27] I. Stavarache, M. L. Ciurea, J. Optoelectron. Adv. Mater. **9**, 2644 (2007).

[28] V. Iancu, M. Draghici, L. Jdira, M. L. Ciurea, J. Optoelectron. Adv. Mater. **6**, 53 (2004).

[29] A.-M. Lepadatu, E. Rusnac, I. Stavarache, Proc. IEEE CN 07TH8934, Int. Semicon. Conf. CAS 2007, Vol. **2**, 575 (2007).